AMERICAN SOCIETY FOR MICROBIOLOGY | Antimicrobial Agents and Chemotherapy®

ANTIVIRAL AGENTS

Zika Virus Replication Is Substantially Inhibited by Novel Favipiravir and Interferon Alpha Combination Regimens

Camilly P. Pires de Mello,[a] Xun Tao,[b] Tae Hwan Kim,[b] Jürgen B. Bulitta,[b] Jaime L. Rodriquez,[a] Justin J. Pomeroy,[a] Ashley N. Brown[a]

[a]Institute for Therapeutic Innovation, Department of Medicine, College of Medicine, University of Florida, Orlando, Florida, USA

[b]Center for Pharmacometrics and Systems Pharmacology, Department of Pharmaceutics, College of Pharmacy, University of Florida, Orlando, Florida, USA

ABSTRACT Zika virus (ZIKV) is a major public health concern due to its overwhelming spread into the Americas. Currently, there are neither licensed vaccines nor antiviral therapies available for the treatment of ZIKV. We aimed to identify and rationally optimize effective therapeutic regimens for ZIKV by evaluating the antiviral potentials of the approved broad-spectrum antiviral agents favipiravir (FAV), interferon alpha (IFN), and ribavirin (RBV) as single agents and in combinations. For these studies, Vero cells were infected with ZIKV in the presence of increasing concentrations of FAV, IFN, or/and RBV for 4 days. Supernatants were harvested daily, and the viral burden was quantified by a plaque assay on Vero cells. The time course of the viral burden during treatment *in vitro* was characterized by a novel translational, mechanism-based model, which was subsequently used to rationally optimize combination dosage regimens. The combination regimen of FAV plus IFN provided the greatest extent of viral inhibition without cytotoxicity, reducing the viral burden by 4.4 $\log_{10}$ PFU/ml at concentrations of 250 μM FAV and 100 IU/ml IFN. Importantly, these concentrations are achievable in humans. The translational, mechanism-based model yielded unbiased and reasonably precise curve fits. Simulations with the model predicted that clinically relevant regimens of FAV plus IFN would markedly reduce viral burdens in humans, resulting in at least a 10,000-fold reduction in the amount of the virus during the first 4 days of treatment. These findings highlight the substantial promise of rationally optimized combination dosage regimens of FAV plus IFN, which should be further investigated to combat ZIKV.

KEYWORDS combination therapy, favipiravir, Zika virus, antiviral agents, interferon alpha, mechanism-based modeling, ribavirin

Zika virus (ZIKV), a mosquito-borne flavivirus, emerged in the Western Hemisphere in 2015 and has since spread explosively throughout the Americas. Serious and long-term health consequences have been associated with infection during recent outbreaks; this applies especially during pregnancy, where devastating birth defects such as microcephaly, brain damage, and fetal loss have been reported (1, 2). Neurological complications have also been linked to ZIKV infection in adults, including Guillain-Barre syndrome and acute disseminated encephalomyelitis (3, 4).

Currently, there are neither approved vaccines nor any antiviral therapies for the prevention or treatment of ZIKV infections. This lack of available medical countermeasures represents a major challenge in the response to (re)emerging viral infections. Traditionally, available antiviral agents are often used as a first line of defense against (re)emerging viruses to decelerate the spread of infection in a population, thereby providing time for the development of new vaccine candidates or new drugs (5). Since antiviral agents specific for ZIKV do not exist, other therapeutic approaches must be

Received 22 September 2017 **Returned for modification** 24 October 2017 **Accepted** 30 October 2017

Accepted manuscript posted online 6 November 2017

Citation Pires de Mello CP, Tao X, Kim TH, Bulitta JB, Rodriquez JL, Pomeroy JJ, Brown AN. 2018. Zika virus replication is substantially inhibited by novel favipiravir and interferon alpha combination regimens. Antimicrob Agents Chemother 62:e01983-17. https://doi.org/10.1128/AAC.01983-17.

Address correspondence to Ashley N. Brown, Ashley.Brown@medicine.ufl.edu.

C.P.P.D.M. and X.T. contributed equally to this work.

investigated. A promising and tangible strategy is to evaluate the antiviral potential of drugs that are currently approved for other indications (i.e., drug repurposing). As repurposed agents have been extensively studied in humans, detailed information regarding pharmacokinetics (PK), pharmacology, and safety is readily available. Compared to traditional drug development, repurposing can tremendously expedite the clinical availability of novel treatment regimens against ZIKV.

Agents that are active against multiple viruses seem particularly suitable candidates for repurposing as anti-ZIKV therapies. Favipiravir (FAV) (formerly T-705), ribavirin (RBV), and interferon alpha (IFN) are three broad-spectrum antiviral agents that are currently approved for the treatment of other viral diseases. FAV is a polymerase inhibitor that is licensed in Japan to treat influenza, but it has also demonstrated activity against Ebola virus, West Nile virus, and yellow fever virus (6–8). RBV and IFN are effective against a multitude of different RNA and DNA viruses and are currently approved by the Food and Drug Administration as combination therapy for the treatment of hepatitis C virus.

Here, we aimed to evaluate the antiviral activities of FAV, RBV, and IFN as single agents and in two-drug combinations against ZIKV to identify potential therapeutic regimens that will maximize virus suppression. As a second objective, we aimed to characterize the time course of the viral burden for these agents as monotherapies and combination therapies via a novel, translational, mechanism-based mathematical model (MBM). This MBM was subsequently used to rationally optimize clinically relevant combination dosage regimens that accounted for the plasma concentration-time profiles of these antiviral agents in humans. Overall, this translational approach was used to identify, design, and rationally optimize novel antiviral combination dosage regimens that are safe and effective in patients infected with ZIKV.

RESULTS

Antiviral monotherapy evaluations. The antiviral activities of FAV, IFN, and RBV were evaluated against a human ZIKV isolate *in vitro*. As monotherapy, FAV suppressed the production of infectious ZIKV in a dose-dependent manner, and suppression was sustained for the entire duration of the experiment (Fig. 1A). FAV was particularly effective at concentrations of 250 and 500 μM, which delayed virus production by approximately 1 day and reduced peak viral titers by 2.1 $\log_{10}$ PFU/ml and 3.6 $\log_{10}$ PFU/ml, respectively (Fig. 1A). The 50% effective concentration (EC_{50}) estimate (based on a Hill model) for FAV against ZIKV over the 4-day experiment was 316.6 μM (49.74 μg/ml).

IFN also displayed activity against ZIKV but only at concentrations of $>$100 IU/ml (Fig. 1C). ZIKV inhibition (INH) was transient in the regimens utilizing 100 IU/ml and 1,000 IU/ml, as the viral burden increased steadily in these arms and eventually attained peak titers that were similar to that of the control by day 4 posttreatment. Continued suppression was achieved at 10,000 IU/ml of IFN, which inhibited the viral burden by approximately 2. $\log_{10}$ PFU/ml (Fig. 1C). IFN exhibited an EC_{50} of 407.8 IU/ml for ZIKV over 4 days of treatment.

The antiviral activity of RBV against ZIKV was limited. RBV concentrations that were $\leq$10 μg/ml were ineffective and failed to suppress the production of infectious virus (Fig. 1B). Substantial virus inhibition was observed at concentrations of 100 μg/ml and 1,000 μg/ml; however, inhibition was not sustainable, and the viral burden continued to increase in both experimental arms throughout the 4-day experiment. Viral titers in the 100-μg/ml arm were similar to those for the control after 4 days of treatment, while the 1,000-μg/ml regimen further delayed ZIKV replication. The overall EC_{50} for RBV against ZIKV was 121.7 μg/ml. Importantly, RBV exhibited strong cytostatic effects at 1,000 μg/ml and was slightly cytostatic at 100 μg/ml (data not shown), which may explain some of the antiviral activity at these concentrations. Toxicity in uninfected control cells was not observed with FAV or IFN treatment at the highest concentrations evaluated in these studies.

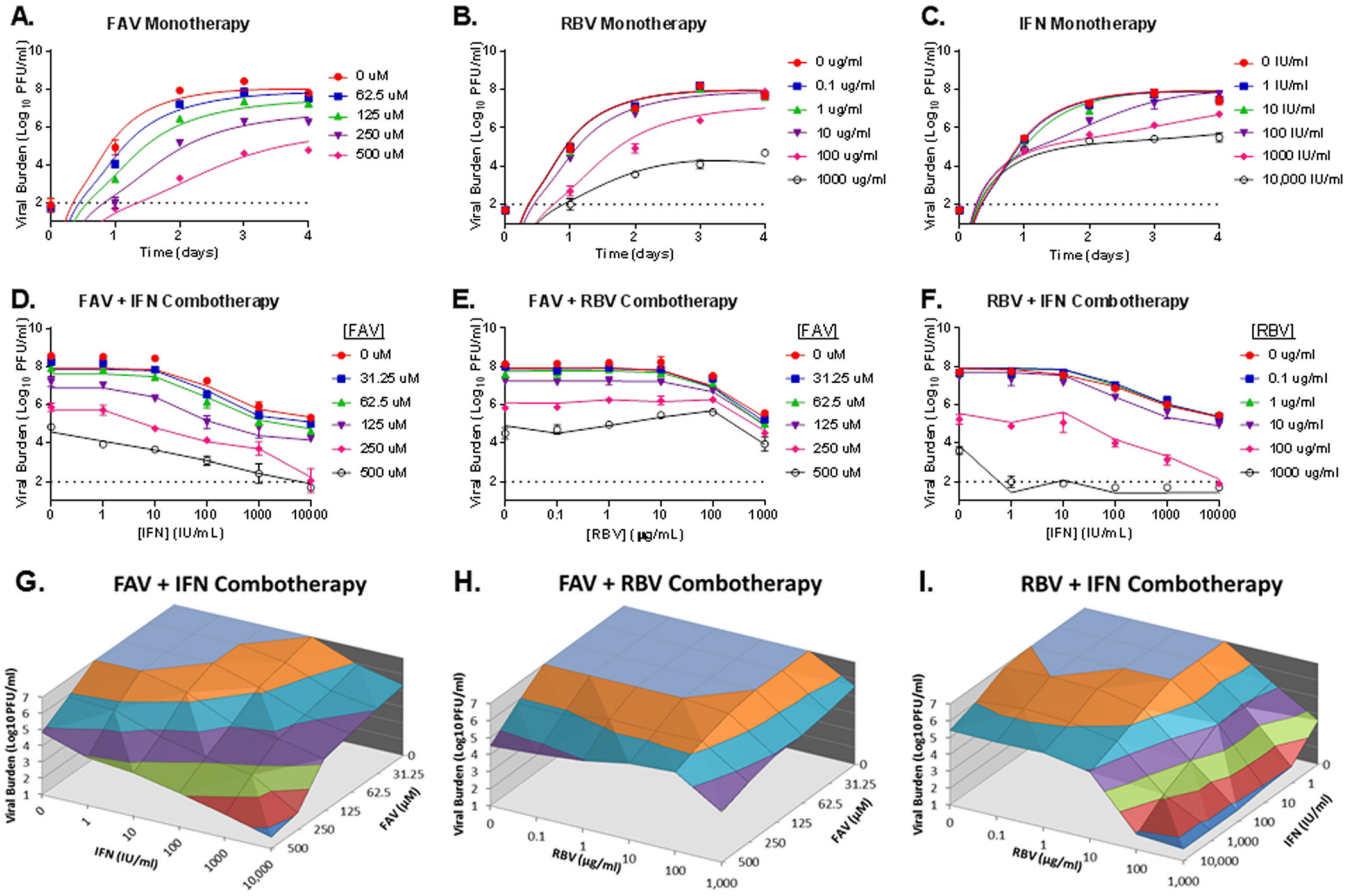

FIG 1 Antiviral activities of favipiravir (FAV), interferon alpha (IFN), and ribavirin (RBV) as monotherapy and combination therapy against Zika virus (ZIKV). (A to C) Vero cells were inoculated with ZIKV at a multiplicity of infection of 0.01 PFU/cell; different concentrations of FAV (A), IFN (B), or RBV (C) were added after infection for single-agent evaluations; and cell culture supernatants were harvested daily. (D to F) For combination evaluations, different concentrations of FAV plus IFN (D), FAV plus RBV (E), or RBV plus IFN (F) were added after inoculation, and cell culture supernatants were sampled on day 3 posttreatment. (G to I) 3D plots illustrating viral burdens for each combination of concentrations are shown for the combinations of FAV plus IFN (G), FAV plus RBV (H), and RBV plus IFN (I). The infectious virus burden, reported as $\log_{10}$ PFU per milliliter, was quantified from cell culture supernatants by a plaque assay on Vero cells. The data are representative of results from one experiment. Data points represent the mean observed viral burdens for three independent samples, and error bars correspond to one standard deviation from three independent samples. Lines through the data points signify the predicted viral burden as determined by the mathematical model. The dashed horizontal line represents the assay limit of detection of 100 PFU/ml.

Antiviral evaluations with combination therapy. We evaluated all possible two-drug combinations of FAV, RBV, and IFN against ZIKV. The combination of FAV and IFN provided substantial virus inhibition, and the degree of inhibition on day 3 was higher than that of either agent as monotherapy (Fig. 1D and G). Moreover, complete virus suppression was observed with 250 μM FAV plus 10,000 IU/ml of IFN as well as 500 μM FAV combined with 1,000 IU/ml or 10,000 IU/ml of IFN. FAV and RBV did not enhance antiviral activity when administered together, as the addition of RBV to FAV yielded viral titers that were similar to those with FAV alone for most regimens (Fig. 1E and H). Importantly, increasing concentrations of RBV decreased virus suppression in regimens containing 500 μM FAV (Fig. 1E and H). The viral burden was lower in experimental arms receiving 1,000 μg/ml of RBV; however, this finding is attributed to RBV-related cytotoxicity. Finally, the effectiveness of RBV plus IFN was higher than that of single-agent therapy but only when high RBV concentrations ($\geq$100 μg/ml) were present (Fig. 1F and I). Regimens containing $\leq$10 μg/ml RBV yielded virus inhibition profiles similar to those observed for IFN monotherapy.

Mechanism-based pharmacodynamic modeling. We developed a novel pharmacodynamic (PD) MBM to describe the relationship between concentrations of FAV, RBV, and IFN as monotherapy and in combination and the production of infectious ZIKV over

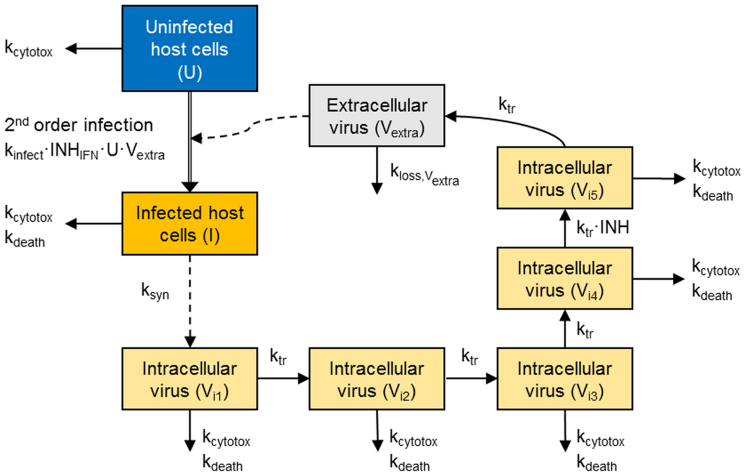

FIG 2 Mechanism-based model for FAV, RBV, and IFN as single-agent therapy and two-drug combinations against ZIKV. The model describes the inhibitory effect of IFN on the infection rate (INH_{IFN}) and the inhibitory effects of FAV and RBV (INH) (which included an antagonism function) on virus maturation in host cells. In addition, RBV cytotoxicity was also demonstrated in the model. FAV and RBV inhibited the transition (k_{tr}) from the 4th to the 5th intracellular virus compartments; an interaction factor was included in this part of the model when FAV and RBV were used in combination.

time. In addition to the antiviral effects of FAV, RBV, and IFN, the MBM (Fig. 2) contained the cytotoxic effects associated with RBV treatment. An antagonistic interaction between FAV and RBV was further required to describe the data (Fig. 1H). The model simultaneously described the viral burdens for all single-agent regimens and two-drug combinations well, as illustrated by the model predictions (depicted as solid lines in Fig. 1A to F). Curve fits were unbiased and precise, with linear regression analysis of fitted-versus-observed plots for viral burdens yielding correlation coefficient (r) values of 0.96 for individual fits and 0.94 for population fits (Fig. 3). The values for the maximum extent of inhibition (I_{max}) for ZIKV production were estimated to be 1.00 for IFN and 0.9999 for FAV, indicating complete or near-complete suppression (Table 1). In contrast, the I_{max} was markedly lower (0.954) for RBV, suggesting that even very high RBV concentrations could not achieve complete virus inhibition. The 50% inhibitory concentration (IC_{50}) estimates were 41.7 μM for FAV, 7.86 μg/ml for RBV, and 4.12 IU/ml

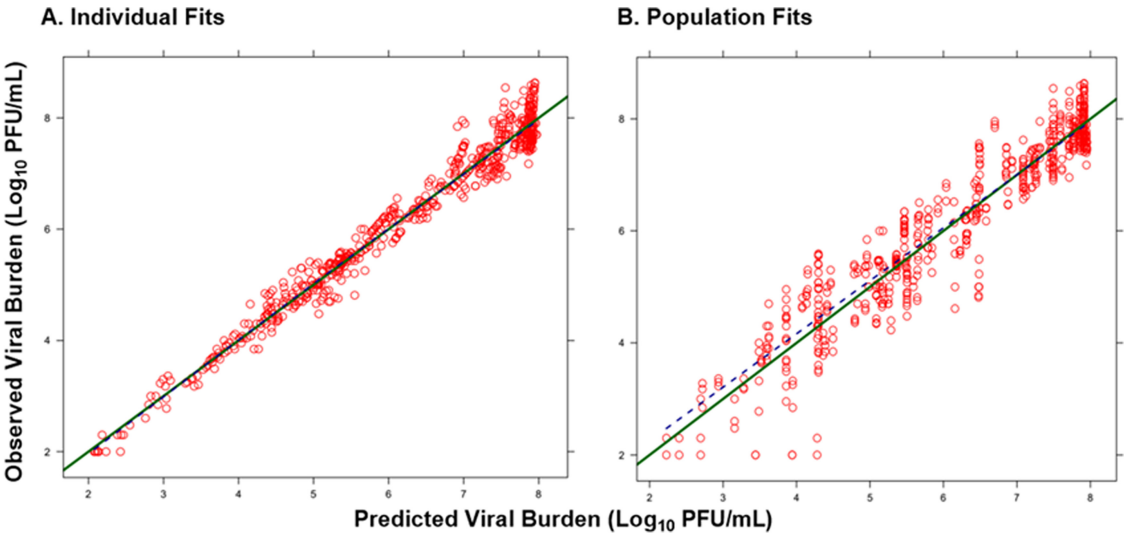

FIG 3 Predicted-versus-observed plots for ZIKV burden. Shown are individual (Bayesian) (A) and population (pre-Bayesian) (B) fitted viral burdens for FAV, RBV, and IFN as monotherapy or combination therapy against ZIKV.

TABLE 1 Parameter estimates for the PD mechanism-based mathematical model of favipiravir, interferon alpha, and ribavirin against Zika virus

Parameter	Symbol (unit of measure)	Population mean estimate (SE [%])	CV[c] of estimate for between-curve variability (SE [%])
PD parameters			
Log_{10} of 2nd-order infection rate constant	k_{infect}	−4.10 (2.39)	0.0841 (128[b])
Synthesis rate constant of virus	k_{syn} (1/h)	9.35 (7.09)	0.068 (219)
Mean delay time until release of virus in the absence of drug	$T_{Delay} = 5/k_{tr}$ (h)	40.0 (2.56)	0.0238 (97)
Mean survival time of infected cells	$MST_{Infected} = 1/k_{death}$ (h)	70.5 (8.92)	0.152 (141)
Mean survival time for extracellular virus	$MST_{Virus} = 1/k_{loss,virus}$ (h)	14.3 (10.4)	0.172 (112)
Log_{10} initial no. of uninfected cells	Log_U	6.30 (fixed)	0 (fixed)
Log_{10} initial no. of infected cells	Log_I	3.38 (2.66)	0.365 (29)
Maximum extent of inhibition by FAV	I_{maxFAV} (normal scale)	0.9999 (~0.9992–1.00[a])	0.793[a] (88.8)
FAV concn causing 50% I_{max}	IC_{50_FAV} (μM)	41.7 (2.55)	0.039 (180)
Hill coefficient of FAV	$Hill_{FAV}$	2.79 (4.53)	0.1 (fixed)
Maximum extent of inhibition by RBV	I_{maxRBV} (normal scale)	0.954 (~0.924–0.973[a])	0.44[a] (120)
RBV concn causing 50% I_{max}	IC_{50_RBV} (μg/ml)	7.86 (9.99)	0.491 (84.3)
Hill coefficient of RBV	$Hill_{RBV}$	2.90 (16.5)	0.1 (fixed)
Maximum extent of inhibition by IFN	I_{maxIFN} (normal scale)	0.99997 (~0.99990–1.00[a])	0.859[a] (62.4)
IFN concn causing 50% I_{max}	IC_{50_IFN} (IU/ml)	4.12 (15.9)	0.131 (383)
Hill coefficient of IFN	$Hill_{IFN}$	2.00 (fixed)	0.1 (fixed)
Interaction factor between FAV and RBV	PSI = 1 if monotherapy, PSI = SYNANT[d] if combination therapy	1.37 (8.21)	0.05 (427)
Maximum extent of cytotoxicity by RBV	$MST_{TOX} = 1/S_{maxRBV}$ (h)	11.9 (7.21)	0.354 (39.3)
RBV concn causing 50% S_{max}	SC_{50_RBV} (μg/ml)	150 (11.3)	0.226 (110)
Hill coefficient of RBV for toxicity	$Hill_{RBVTOX}$ (normal scale)	4.16 (12.5)	0.1 (fixed)
Residual-error parameter			
Additive error for viral load on log_{10} scale	SDin	0.333 (4.67)	

[a] I_{max} was assumed to be normally distributed on a logistically transformed scale ($I_{maxTransformed}$). The population mean value of I_{max} is reported on a normal scale (i.e., from 0 to 1), whereas the between-curve variability is presented as the standard deviation of a normal distribution on a logistically transformed scale.

[b] Between-curve variability was included and required in this population PD model to account for minor biological differences between experimental curves on separate days. The uncertainty (percent standard error) for the estimated between-curve variability tended to be large for some parameters. However, this has only a minor or no effect on the predictive performance of the model, as shown by the NPDE.

[c] CV, coefficient of variation.

[d] SYNANT, synergy or antagonism.

for IFN. It should be noted that the model IC_{50} estimates refer to the suppression of the release of infectious ZIKV from the final intracellular virus compartment and that these estimates are different from the EC_{50}s (based on an empirical Hill model) reported above. The EC_{50} instead correlates the drug concentration to the overall viral burden quantified by the plaque assay.

The substantial inhibition of virus production by the combination of FAV and IFN was well described by the MBM; excitingly, the viral burden was decreased by approximately 4.5 log_{10} units relative to the no-treatment controls at 250 μM FAV with 100 IU/ml of IFN. More importantly, the exposures associated with these concentrations are clinically achievable (9, 10). Extensive virus suppression was also observed with RBV in combination with IFN but only when high levels of RBV were present ($\geq$100 μg/ml). Since the estimated 50% cytotoxicity concentration (SC_{50_RBV}) for RBV was 150 μg/ml (Table 1), the effectiveness of this regimen was attributed mainly to the considerable cytotoxicity associated with RBV treatment. In contrast, FAV and RBV in combination demonstrated less-than-additive interactions for an antiviral effect. The estimated interaction factor was 1.37 (Table 1), which indicated antagonism ($P < 0.001$ [likelihood ratio test] in comparison to a model without an interaction factor). Antagonism was most apparent with FAV at 500 μM and RBV at 100 μg/ml (Fig. 1E and H).

Predictive performance. The normalized prediction distribution error (NPDE) is well known to be a statistically rigorous method to assess predictive performance. This plot suggested a good predictive performance of the proposed final model, with approximately 95% of markers falling symmetrically within the ideal range of −2 to +2 for standard normally distributed variables (Fig. 4). This suggested a suitable predictive performance of the proposed model for subsequent use in simulations.

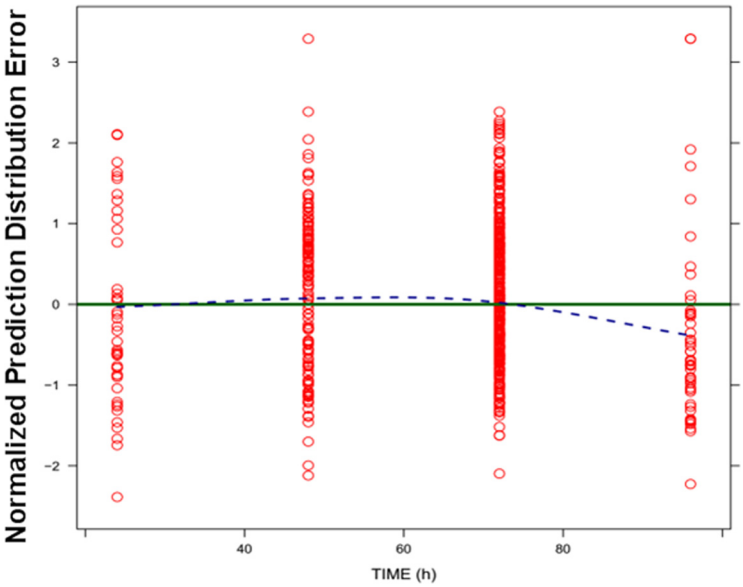

FIG 4 Normalized prediction distribution error (NPDE) for viral burden. The NPDE should ideally have a standard normal distribution with 95% of the points ranging between −2 and +2 at each time point.

Simulations of combination therapy with FAV and IFN against ZIKV. Our results suggested that FAV in combination with IFN was the most promising regimen for the treatment of ZIKV. Based on our translational MBM, antiviral activity against ZIKV for combination therapy with FAV and IFN was predicted for clinically relevant dosage regimens. Human PK profiles associated with clinically relevant regimens of FAV administered orally were evaluated in combination with a standard clinical regimen of injected IFN at 36 million IU/ml twice daily (9) (Fig. 5A and B). PK profiles were corrected for protein binding, and only free-drug concentrations were used in the simulations. Two FAV regimens that have been used clinically were evaluated in this study: (i) the standard regimen used for the treatment of human influenza virus infections in phase 3 clinical trials in the United States (1,800 mg at 0 and 12 h on day 1, followed by 800 mg every 12 h starting at 24 h), which we termed the low-dose regimen (ClinicalTrials registration number NCT02008344), and (ii) a clinical regimen that was used to treat Ebola virus-infected patients during the 2014 outbreak (2,400 mg at 0 h, 2,400 mg at 8 h, and 1,800 mg at 16 h on day 1, followed by 1,200 mg every 12 h starting at 24 h), referred to as the high-dose regimen (11). We also assessed a third FAV regimen that employed doses that were between those of the low- and high-dose regimens (1,800 mg at 0, 8, and 16 h on day 1, followed by 900 mg every 12 h starting at 24 h). This treatment was designated the middle-dose regimen (Fig. 5B).

In the absence of treatment, our simulations showed that the ZIKV burden achieved peak viral titers of 8 $\log_{10}$ PFU/ml (Fig. 5C and D). As monotherapy, FAV decreased peak ZIKV titers relative to the control by 1.2 $\log_{10}$ units for the low-dose regimen, 1.5 $\log_{10}$ units for the middle-dose regimen, and 1.9 $\log_{10}$ units for the high-dose regimen (Fig. 5C). FAV treatment also delayed the achievement of peak viral titers by approximately 3 days. IFN as monotherapy delayed ZIKV production but was unable to suppress viral replication, as peak viral titers were similar to those of the control by day 5 (Fig. 5C).

Simulations with all combination treatment regimens yielded substantial virus suppression relative to monotherapy, and the degree of suppression occurred in a dose-dependent manner (Fig. 5D). All regimens markedly inhibited the ZIKV burden relative to the control, especially at the earlier time points; however, the viral burden increased only slowly over the course of the 10-day simulation, indicating that these regimens were effective at delaying ZIKV production (Fig. 5D). After 10 days of treatment, the model predicted that the low-dose regimen in combination with IFN

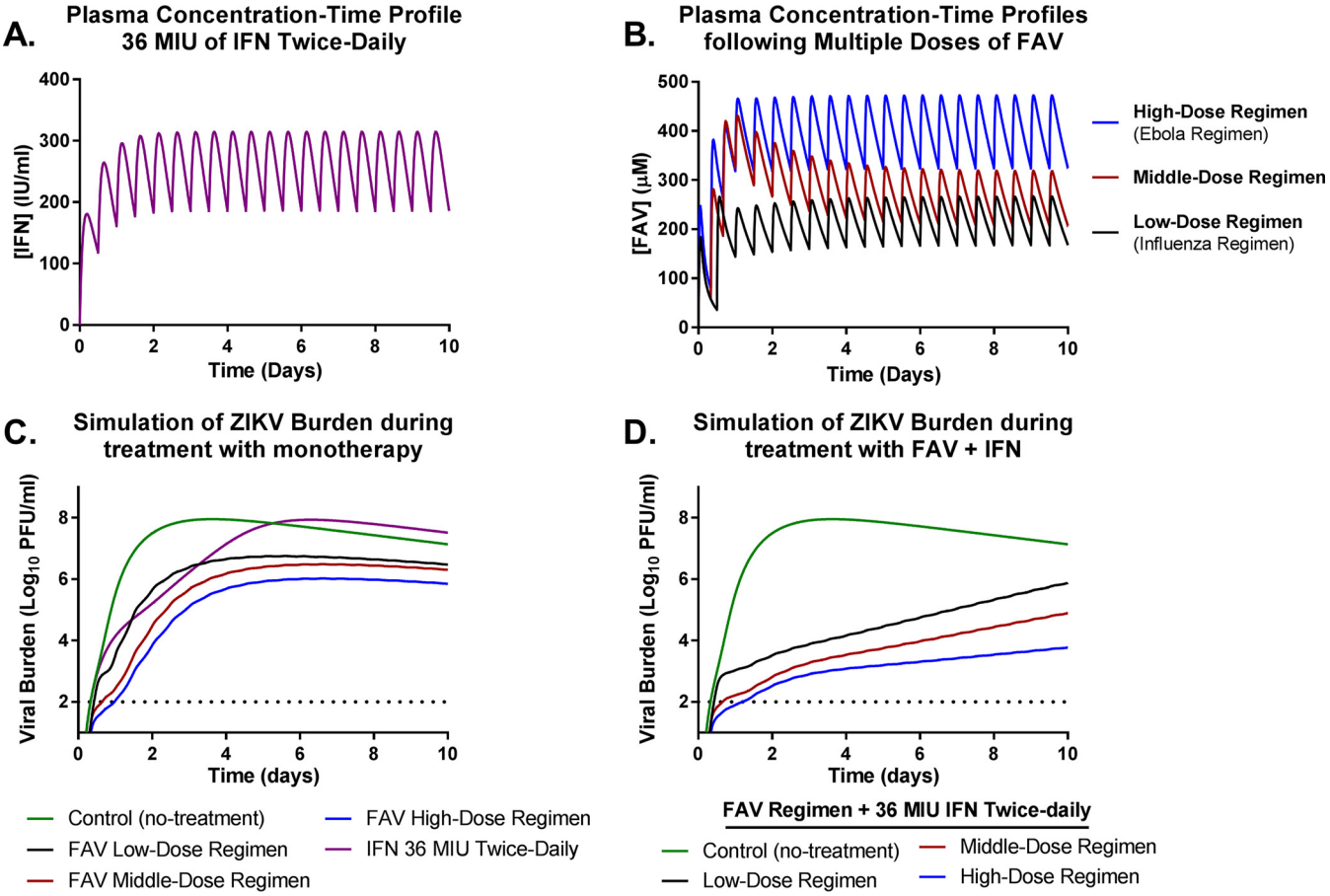

FIG 5 Simulations of antiviral activities of clinically relevant regimens of IFN and FAV in combination against ZIKV. (A and B) Human plasma concentration-time profiles associated with the standard clinical regimen of 36 million international units (MIU) of IFN administered via injection (A) and clinically utilized regimens for orally administered FAV (B). The low-dose regimen refers to the standard FAV regimen used to treat human influenza virus infections, which is in phase 3 clinical trials in the United States. The high-dose regimen corresponds to the FAV regimen employed to treat humans infected with Ebola virus. The middle-dose regimen was selected because it employs drug levels that were between the low- and high-dose regimens. (C) ZIKV burden resulting from treatment with the high-, medium-, and low-FAV regimens or the IFN regimen as monotherapy. (D) ZIKV burden during treatment with regimens of IFN plus FAV, as predicted by the mechanism-based mathematical model. The dashed horizontal line at $y = 2$ $\log_{10}$ units corresponds to the limit of detection of the plaque assay that was used to quantify viral burdens in the experimental assays.

would inhibit the viral burden by 2.1 $\log_{10}$ PFU/ml, the middle-dose regimen would decrease the viral load by 3.1 $\log_{10}$ PFU/ml, and the high-dose regimen would decrease the viral load by 4.2 $\log_{10}$ PFU/ml.

DISCUSSION

The rapid spread of ZIKV throughout the Americas coupled with the serious neurologic symptoms associated with this disease underscore the urgent need to identify effective medical countermeasures against ZIKV. Although vaccination is traditionally a cornerstone for the prevention of viral diseases, recent studies have called into question the safety of an anti-ZIKV vaccine due to concerns of antibody-dependent enhancement; the latter may exacerbate infections caused by other flaviviruses (i.e., dengue virus) (12). This is a significant shortcoming, since multiple flaviviruses cocirculate geographically and are transmitted by the same mosquito vector (13). Consequently, optimal antiviral therapy will play a significant role in the management of ZIKV infections. Antiviral agents specific for ZIKV do not currently exist. Here, we applied a drug-repurposing strategy to identify effective therapeutic regimens for ZIKV by evaluating approved agents that have broad-spectrum antiviral activity. In addition to single-agent evaluations, compounds were also assessed in combination to maximize viral suppression. Finally, we developed a novel MBM to predict the effectiveness of

clinically relevant antiviral regimens when human PK profiles associated with these regimens are simulated.

Our experimental assays and MBM showed that antiviral treatment with two compounds yielded superior virologic outcomes compared to those with single-agent therapy. When FAV was combined with IFN, this combination demonstrated substantial ZIKV suppression without exhibiting cytotoxicity to uninfected host cells. More importantly, considerable antiviral effectiveness was observed at clinically relevant FAV and IFN concentrations. These findings strongly support the further investigation of FAV and IFN as a combination treatment against ZIKV.

The addition of IFN to RBV also enhanced antiviral activity, resulting in extensive virus suppression compared to monotherapy. However, suppression occurred only with regimens that contained high levels of RBV, which are not achievable in humans due to toxicity, thereby limiting the potential clinical utility of this treatment regimen. The combination of FAV and RBV demonstrated statistically significant antagonism using a competitive-interaction model as the null reference model (14). We hypothesize that these antagonistic interactions for virus suppression stem from the potential overlap in the mechanism(s) of action between FAV and RBV, as both of these compounds may act as purine analogs to inhibit viral replication (15–17). Antagonism was most obvious when 500 μM FAV was combined with 100 μg/ml of RBV; the latter was the highest concentration of RBV that did not yield extensive cytotoxicity. We postulate that at these concentrations, RBV was outcompeting FAV for utilization by the ZIKV RNA-dependent RNA polymerase during viral replication. Since RBV has substantially lower virus inhibition than FAV (I_{max} value of 0.954 for RBV, compared to 0.9999 for FAV), the overall degree of ZIKV suppression by RBV was limited. Thus, these findings demonstrate that FAV in combination with RBV is not an optimal regimen to pursue for the treatment of human ZIKV infections.

Our experimental assays were conducted by using static concentrations of each compound. In humans, plasma concentration-time profiles for agents are dynamic after administration according to each drug's PK. We conducted simulations with our novel MBM using clinically relevant PK profiles for FAV and IFN in combination to predict the antiviral effectiveness of various regimens against ZIKV in humans. Our simulations showed that all combination regimens substantially inhibited ZIKV production over a 10-day period. The maximum extent of virus inhibition was achieved when the high-dose FAV regimen that was used to treat Ebola virus-infected patients was combined with the standard clinical dose of IFN, suppressing the viral burden by over 15,000-fold. It is important to note that our studies and analyses do not account for the human immune response. Therefore, our findings may underpredict antiviral activity, and additional suppression may be achieved in the presence of a functioning immune system. The implications for this are significant, as the antiviral effectiveness provided by the clinical regimen of IFN plus a low-dose FAV regimen may be sufficient to allow the immune system to clear the remaining infection; this low-dose FAV regimen was used in influenza virus clinical trials (ClinicalTrials registration number NCT02008344).

Despite the promising antiviral activity of the combination treatment of IFN and FAV, there are weaknesses associated with this therapeutic regimen. First, FAV has demonstrated teratogenic and embryotoxic effects in many different animal models, including monkeys (18); thus, FAV is contraindicated for pregnant women and cannot be utilized for protection against microcephaly or other birth defects associated with ZIKV infection during pregnancy. Additionally, the ability of FAV to penetrate into the central nervous system of humans is unknown, and others have shown that IFN does not efficiently cross the blood-brain barrier (19). This suggests that FAV plus IFN may not protect against the neurologic disease resulting from ZIKV in adults. However, antiviral intervention with FAV and IFN has the potential to control ZIKV in peripheral tissues, which may in turn prevent or decrease the severity of neurologic consequences occurring with infection. FAV is detected in semen (18), a site where ZIKV has been shown to persist for many months (20, 21). There is also evidence that systemic IFN penetrates into seminal fluid (22). Therefore, FAV plus IFN may be effective at control-

ling ZIKV infection in human sexual organs and, as a result, help to prevent sexual transmission of the virus to uninfected partners.

There are several limitations to our study. First, the available information regarding human PK for FAV was sparse (10). Our PK simulations were based on mean concentration profiles for healthy volunteers. Although these PK data allowed us to simulate the average exposure in humans, we could not include between-patient variability since population PK models for FAV and IFN were not available. Also, the PK in patients with ZIKV may differ from those in healthy volunteers. As more information becomes accessible, we will be able to more accurately simulate FAV PK profiles and account for between-patient variability in a population. Second, our evaluations relied on FAV concentrations and not the concentrations of the active intracellular triphosphorylated moiety. We are currently investigating the intracellular phosphorylation kinetics of FAV in different host cells and will incorporate these findings into a future MBM. Finally, our evaluations were conducted on a single ZIKV isolate. Although the isolate that we employed represents a contemporary human ZIKV isolate, future experiments will focus on assessing antiviral combination regimens against multiple strains of ZIKV in different host cell lines.

In conclusion, our study demonstrated that clinically relevant FAV and IFN combination regimens have great potential as a treatment strategy for ZIKV infections. These encouraging findings suggest that further preclinical studies (including animal models) and, ultimately, clinical investigations of the combination of FAV plus IFN are warranted.

MATERIALS AND METHODS

Cells and compounds. Vero cells (ATCC CCL-81, American Type Culture Collection, Manassas, VA) were cultured in Eagle's minimum essential medium (MEM) (Cellgro; Corning, Manassas, VA) in the presence of 5% fetal bovine serum (FBS; Sigma-Aldrich, St. Louis, MO) and a 1% penicillin-streptomycin solution (HyClone, Logan City, UT) at 37°C in 5% CO_2. Cells were passaged twice weekly via trypsin digestion to maintain subconfluent cell monolayers.

FAV, RBV, and IFN were purchased from commercial vendors. FAV was obtained from Cellagen Technology (San Diego, CA), RBV was obtained from Tokyo Chemical Industry (Portland, OR), and IFN was obtained from PBL Assay Science (Piscataway, NJ). All three compounds were stored according to the manufacturers' recommendations.

Virus. The 2015 human ZIKV Puerto Rican strain PRVABC59 was acquired from BEI Resources (Manassas, VA). Virus stocks were generated by passing the ZIKV isolate on Vero cells. Cell supernatants were collected 3 days after infection and clarified by high-speed centrifugation. The virus was aliquoted and frozen at −80°C in the presence of 20% FBS. Stock viral titers were determined by a plaque assay on Vero cells.

ZIKV plaque assay. Supernatant samples were thawed at 37°C and then stored on ice. Samples were diluted serially 10-fold in MEM containing 2% FBS, and a 100-μl aliquot of each dilution was then added to confluent Vero cell monolayers in 6-well plates. The virus was allowed to attach to cells for 1 h at 37°C in 5% CO_2. After the 1-h incubation period, 3 ml of a primary MEM agar overlay containing a final concentration of 0.6% agar and 5% FBS was added to all wells. A second MEM agar overlay supplemented with a final concentration of 1% agar, 1% FBS, 200 μg/ml of DEAE-dextran, and 0.008% neutral red was added to each well 3 days later. Plaques were counted 24 h after the addition of the second agar overlay. The viral burden is reported as PFU per milliliter.

Antiviral evaluations. The antiviral activities of FAV, IFN, and RBV against ZIKV were evaluated on Vero cells in triplicate, as previously described (23), with the exception that ZIKV was inoculated onto confluent Vero cell monolayers at a multiplicity of infection of 0.01 PFU/cell. FAV was evaluated at concentrations ranging from 0 μM to 500 μM, RBV was evaluated at concentrations ranging from 0 μg/ml to 1,000 μg/ml, and IFN was evaluated at concentrations ranging from 0 IU/ml to 10,000 IU/ml. For single-agent evaluations, cell supernatants were harvested daily, clarified by high-speed centrifugation, and frozen at −80°C until the end of the experiment. The infectious virus burdens for all samples were quantified simultaneously by a plaque assay on Vero cells. The EC_{50} value for each compound was determined over the entire time course of the study by using GraphPad Prism software (La Jolla, CA). Briefly, the area under the viral burden-time curve (AUC_{viral_burden}) was calculated for all treatment regimens (Fig. 1A to C), and an inhibitory sigmoid-E_{max} model was fit to the AUC_{viral_burden} values. Each assay was conducted in triplicate.

Combination assays were performed with FAV, IFN, and RBV by using a 6-by-6 checkerboard format in which 5 concentrations of each drug with a no-treatment control were assessed alone and as all possible combinations of concentrations, resulting in 36 assay points. Each assay was conducted in triplicate. Supernatants were harvested on day 3 posttreatment, as peak viral burdens were achieved at this time point in all previous time course analyses. Samples were processed as described above and quantified for infectious virus by a plaque assay.

Mechanism-based pharmacodynamic mathematical model. A new MBM was developed to investigate the inhibitory effects of FAV, RBV, and IFN as monotherapy as well as of all 2-drug combinations of these compounds on viral replication. The virus and cells were exposure to a range of concentrations of the above-mentioned three drugs. The model contained compartments for uninfected and infected host cells as well as extracellular and intracellular virus.

Host cell dynamics. Uninfected host cells (U) were infected by extracellular virus (V_{extra}) via a second-order process with the infection rate constant k_{infect}. IFN inhibited the infection. In our *in vitro* experiments, uninfected and infected (I) host cells were assumed not to replicate. Infected host cells died via a first-order process (death rate constant k_{death}), which was stimulated by a minor cytotoxic effect of FAV at high concentrations. Cytotoxicity by RBV affected both uninfected and infected host cells. The differential equations for U and I were

$$\frac{dU}{dt} = -k_{infect} \times INH_{IFN} \times V_{extra} \times U - k_{cytotox} \times U \qquad IC,\ 10^{6.3}\ cells \tag{1}$$

$$\frac{dI}{dt} = k_{infect} \times INH_{IFN} \times V_{extra} \times U - \left(k_{death} + k_{cytotox}\right) \times I \qquad IC,\ \log_{10}Inoc_I \tag{2}$$

The initial condition (IC) was set to the targeted inoculum of $10^{6.3}$ cells/ml for total uninfected host cells and estimated for infected host cells. The cytotoxicity ($k_{cytotox}$) by RBV is described below.

Viral replication. After host cells were infected, new intracellular virus (V_{i1}) was generated with a first-order synthesis rate constant (k_{syn}). Based on our previously developed mechanism-based model, a series of five transit compartments for intracellular virus (V_{i1}, V_{i2}, V_{i3}, V_{i4}, and V_{i5}, linked by transit rate constant k_{tr}) was used to describe virus maturation and replication (24). Differential equations for intracellular virus were as follows (initial conditions of V_{i1} to V_{i5} all zero):

$$\frac{dV_{il}}{dt} = k_{syn} \times I - k_{tr} \times V_{il} - \left(k_{death} + k_{cytotox}\right) \times V_{il} \tag{3}$$

$$\frac{dV_{i2}}{dt} = k_{tr} \times \left(V_{i1} - V_{i2}\right) - \left(k_{death} + k_{cytotox}\right) \times V_{i2} \tag{4}$$

$$\frac{dV_{i3}}{dt} = k_{tr} \times \left(V_{i2} - V_{i3}\right) - \left(k_{death} + k_{cytotox}\right) \times V_{i3} \tag{5}$$

$$\frac{dV_{i4}}{dt} = k_{tr} \times \left(V_{i3} - V_{i4} \times INH_{FAV} \text{ or } INH_{RBV}\right) - \left(k_{death} + k_{cytotox}\right) \times V_{i4} \tag{6}$$

$$\frac{dV_{i5}}{dt} = k_{tr} \times \left(V_{i4} \times INH_{FAV} \text{ or } INH_{RBV} - V_{i5}\right) - \left(k_{death} + k_{cytotox}\right) \times V_{i5} \tag{7}$$

The death of infected host cells caused a loss of the associated immature intracellular virus. Therefore, cytotoxicity by RBV, for example, caused the death of infected host cells and the loss of intracellular virus as described by k_{death} in the differential equations for V_{i1} to V_{i5}.

Extracellular virus (V_{extra}) arose from the egress of intracellular virus from compartment V_{i5} and was subject to a first-order loss rate constant ($k_{loss,}V_{extra}$). At the initiation of our *in vitro* experiment, all extracellular virus was assumed to rapidly infect host cell, and thus, the initial condition for V_{extra} was set to zero. The different equation was

$$\frac{dV_{extra}}{dt} = k_{tr} \times V_{i5} - k_{loss,V_{extra}} \times V_{extra} \qquad IC,\ 0\ \ PFU/ml \tag{8}$$

Drug effect. IFN exhibits an antiviral effect by binding to IFN receptors on the cell surface, which induces an antiviral state within that cell. This cellular antiviral state prevents viral infection in uninfected cells. IFN inhibits cellular infection by an inhibitory Hill function with maximum extent of inhibition (I_{maxIFN}) and the IFN concentration causing 50% I_{max} (IC_{50_IFN}). The coefficient for IFN ($Hill_{IFN}$) was fixed as 2, informed by IFN monotherapy modeling (results not shown):

$$INH_{IFN} = 1 - I_{max\ IFN} \times \frac{C_{IFN}{}^{Hill_{IFN}}}{C_{IFN}{}^{Hill_{IFN}} + IC_{50\_IFN}{}^{Hill_{IFN}}} \tag{9}$$

FAV and RBV inhibit the replication of viral RNA in infected host cells. Their effect was modeled as the inhibition of transit from compartment V_{i4} to compartment V_{i5} by an inhibitory Hill function. The maximum extent of inhibition ($I_{max\ FAV}$) and FAV concentrations causing 50% $I_{max\ FAV}$ (IC_{50_FAV}) and the respective parameters for RBV were estimated:

$$INH_{FAV} = 1 - I_{max\ FAV} \times \frac{C_{FAV}{}^{Hill_{FAV}}}{C_{FAV}{}^{Hill_{FAV}} + IC_{50\_FAV}{}^{Hill_{FAV}}} \tag{10}$$

$$INH_{RBV} = 1 - I_{max\ RBV} \times \frac{C_{RBV}{}^{Hill_{RBV}}}{C_{RBV}{}^{Hill_{RBV}} + IC_{50\_RBV}{}^{Hill_{RBV}}} \tag{11}$$

Additionally, RBV resulted in cytotoxicity for both uninfected and infected host cells; this was modeled via a stimulatory Hill equation with the maximum extent of stimulation ($S_{max\ RBV}$) and the RBV concentration (SC_{50_RBV}) causing 50% $S_{max\ RBV}$:

$$k_{cytotox} = S_{max\ RBV} \frac{C_{RBV}{}^{Hill_{RBVTOX}}}{C_{RBV}{}^{Hill_{RBVTOX}} + SC_{50\_RBV}{}^{Hill_{RBVTOX}}} \tag{12}$$

Synergy and antagonism. The observed virus concentrations at 72 h were plotted against the concentrations of 2 drugs to create three-dimensional (3D) surface plots for each 2-drug combination. Synergy or antagonism at different concentration regions was assessed by comparing the surface plots for the observed and predicted virus concentrations. The modeled additive surface was defined by the model predictions with each drug acting independently (i.e., without an interaction factor) via the effects shown above.

In this model, the combinations of IFN plus FAV and IFN plus RBV have the potential to achieve substantial inhibition of viral replication, since IFN inhibits upstream infection of host cells, and FAV or RBV inhibits the downstream virus maturation process. As designed by the mechanism-based model structure, the combination of these two effects can yield clinically relevant synergy of virus suppression, even though these two combinations contain no interaction factor.

We considered models with antagonism between FAV and RBV. Antagonism was empirically described by an interaction factor (PSI) via a competitive-interaction model (14). For the model with antagonism, the individual effects of FAV and RBV were replaced by the joint effect of INH:

$$\mathrm{INH} = 1 - \frac{I_{\mathrm{maxFAV}} \times \left[C_{\mathrm{FAV}}/\left(\mathrm{PSI} \times \mathrm{IC}_{50\_\mathrm{FAV}}\right)\right]^{\mathrm{Hill}_{\mathrm{FAV}}} + I_{\mathrm{maxRBV}} \times \left[C_{\mathrm{RBV}}/\left(\mathrm{PSI} \times \mathrm{IC}_{50\_\mathrm{RBV}}\right)\right]^{\mathrm{Hill}_{\mathrm{RBV}}}}{\left[C_{\mathrm{FAV}}/\left(\mathrm{PSI} \times \mathrm{IC}_{50\_\mathrm{FAV}}\right)\right]^{\mathrm{Hill}_{\mathrm{FAV}}} + \left[C_{\mathrm{RBV}}/\left(\mathrm{PSI} \times \mathrm{IC}_{50\_\mathrm{RBV}}\right)\right]^{\mathrm{Hill}_{\mathrm{RBV}}} + 1} \quad (13)$$

System outputs and residual-error model. The model contained $\log_{10}$ PFU per milliliter as the dependent variable. In the plaque assay, each extracellular virus forms one plaque that is counted as described above. To account for samples below the quantification limit for the plaque assay at time zero, the Beal M3 method (25) was used for PD modeling. We used an additive residual error on a $\log_{10}$ scale for the data for PFU per milliliter.

Parameter variability model. A standard exponential parameter variability model was used for most of the parameters. A logistic transformation was employed to constrain the individual I_{max} estimates between 0 and 1. The I_{max} was assumed to be normally distributed on a logistically transformed scale. Normal distributions were also employed for parameters estimated on a log scale (i.e., for Log_U and Log_I [log-transformed uninfected and infected host cells, respectively]).

Model qualification. Individual curve fit plots over time, individual and population fitted-versus-observed plots, and NPDE plots were used to assess the goodness of fit and predictive performance. Models were compared based on standard diagnostic plots, the objective function (negative log likelihood), and the plausibility of PD parameter estimates.

PK modeling. To simulate clinically relevant concentrations, we developed PK models for FAV and IFN. These models were combined with the PD model (described above) to predict antiviral activities of various drug dosage regimens in humans. A full description of the developed PK models is shown in the supplemental material.

FAV PK model. The observed PK data for FAV after repeated doses in Japanese volunteers were digitized from previously reported figures (10). The PK model contained first-order absorption, and systemic disposition was described by one disposition compartment. In that report, the systemic clearance of FAV was found to be significantly decreased over time. Similar PK properties were also observed in preclinical studies, and these properties were explained by enzyme-mediated elimination with concentration-dependent inhibition (26). Thus, we adapted a previously developed PK model for the autoinhibition of FAV clearance during repeated administration (27).

IFN PK model. The observed PK data for IFN obtained after intramuscular injection in cancer patients were digitized (9). Since the PK was linear over the dosage range studied (from 3 million to 198 million IU), systemic disposition of IFN was described by a linear one-compartment model. The administered IFN was described by first-order kinetics.

Software and algorithm. For estimation of the PD model parameters and of the PK models, we used the Monte Carlo parametric expectation maximization (MC-PEM) (also called importance sampling) algorithm in the parallelized software S-ADAPT (version 1.57). The SADAPT-TRAN facilitator tool was employed (28).

Simulations for the combined PK/PD model. Simulations were performed with Berkeley Madonna (version 8.23.3.0) software. The concentration-time profiles of FAV and IFN were simulated for clinically relevant dosage regimens. Simulated PK profiles were used as input functions for the drug effects in the PD model. In addition, host cell turnover was considered via a sensitivity analysis for these simulations to mimic a range of physiological conditions.

SUPPLEMENTAL MATERIAL

Supplemental material for this article may be found at https://doi.org/10.1128/AAC.01983-17.

SUPPLEMENTAL FILE 1, PDF file, 0.1 MB.

ACKNOWLEDGMENTS

This work was supported by grant 7ZK30 from the Florida Department of Health, Biomedical Research Program. The funders had no role in study design, data collection and interpretation, or the decision to submit the work for publication. We declare no competing interests.

REFERENCES

1. Kleber de Oliveira W, Cortez-Escalante J, De Oliveira WT, do Carmo GM, Henriques CM, Coelho GE, Araujo de Franca GV. 2016. Increase in reported prevalence of microcephaly in infants born to women living in areas with confirmed Zika virus transmission during the first trimester of pregnancy—Brazil, 2015. MMWR Morb Mortal Wkly Rep 65:242–247. https://doi.org/10.15585/mmwr.mm6509e2.
2. Cauchemez S, Besnard M, Bompard P, Dub T, Guillemette-Artur P, Eyrolle-Guignot D, Salje H, Van Kerkhove MD, Abadie V, Garel C, Fontanet A, Mallet HP. 2016. Association between Zika virus and microcephaly in French Polynesia, 2013-15: a retrospective study. Lancet 387:2125–2132. https://doi.org/10.1016/S0140-6736(16)00651-6.
3. Cao-Lormeau VM, Blake A, Mons S, Lastere S, Roche C, Vanhomwegen J, Dub T, Baudouin L, Teissier A, Larre P, Vial AL, Decam C, Choumet V, Halstead SK, Willison HJ, Musset L, Manuguerra JC, Despres P, Fournier E, Mallet HP, Musso D, Fontanet A, Neil J, Ghawche F. 2016. Guillain-Barre syndrome outbreak associated with Zika virus infection in French Polynesia: a case-control study. Lancet 387:1531–1539. https://doi.org/10.1016/S0140-6736(16)00562-6.
4. Broutet N, Krauer F, Riesen M, Khalakdina A, Almiron M, Aldighieri S, Espinal M, Low N, Dye C. 2016. Zika virus as a cause of neurologic disorders. N Engl J Med 374:1506–1509. https://doi.org/10.1056/NEJMp1602708.
5. Xu M, Lee EM, Wen Z, Cheng Y, Huang WK, Qian X, Tcw J, Kouznetsova J, Ogden SC, Hammack C, Jacob F, Nguyen HN, Itkin M, Hanna C, Shinn P, Allen C, Michael SG, Simeonov A, Huang W, Christian KM, Goate A, Brennand KJ, Huang R, Xia M, Ming GL, Zheng W, Song H, Tang H. 2016. Identification of small-molecule inhibitors of Zika virus infection and induced neural cell death via a drug repurposing screen. Nat Med 22:1101–1107. https://doi.org/10.1038/nm.4184.
6. Julander JG, Shafer K, Smee DF, Morrey JD, Furuta Y. 2009. Activity of T-705 in a hamster model of yellow fever virus infection in comparison with that of a chemically related compound, T-1106. Antimicrob Agents Chemother 53:202–209. https://doi.org/10.1128/AAC.01074-08.
7. Mentre F, Taburet AM, Guedj J, Anglaret X, Keita S, de Lamballerie X, Malvy D. 2015. Dose regimen of favipiravir for Ebola virus disease. Lancet Infect Dis 15:150–151. https://doi.org/10.1016/S1473-3099(14)71047-3.
8. Morrey JD, Taro BS, Siddharthan V, Wang H, Smee DF, Christensen AJ, Furuta Y. 2008. Efficacy of orally administered T-705 pyrazine analog on lethal West Nile virus infection in rodents. Antiviral Res 80:377–379. https://doi.org/10.1016/j.antiviral.2008.07.009.
9. Gutterman JU, Fine S, Quesada J, Horning SJ, Levine JF, Alexanian R, Bernhardt L, Kramer M, Spiegel H, Colburn W, Trown P, Merigan T, Dziewanowski Z. 1982. Recombinant leukocyte A interferon: pharmacokinetics, single-dose tolerance, and biologic effects in cancer patients. Ann Intern Med 96:549–556. https://doi.org/10.7326/0003-4819-96-5-549.
10. Pharmaceuticals and Medical Devices Agency. 2014. Review report. Report on the deliberation results of favipiravir (English version). Pharmaceuticals and Medical Devices Agency, Tokyo, Japan.
11. Nguyen TH, Guedj J, Anglaret X, Laouenan C, Madelain V, Taburet AM, Baize S, Sissoko D, Pastorino B, Rodallec A, Piorkowski G, Carazo S, Conde MN, Gala JL, Bore JA, Carbonnelle C, Jacquot F, Raoul H, Malvy D, de Lamballerie X, Mentre F. 2017. Favipiravir pharmacokinetics in Ebola-infected patients of the JIKI trial reveals concentrations lower than targeted. PLoS Negl Trop Dis 11:e0005389. https://doi.org/10.1371/journal.pntd.0005389.
12. Bardina SV, Bunduc P, Tripathi S, Duehr J, Frere JJ, Brown JA, Nachbagauer R, Foster GA, Krysztof D, Tortorella D, Stramer SL, Garcia-Sastre A, Krammer F, Lim JK. 2017. Enhancement of Zika virus pathogenesis by preexisting antiflavivirus immunity. Science 356:175–180. https://doi.org/10.1126/science.aal4365.
13. Simmons CP, Farrar JJ, Chau NVV, Wills B. 2012. Dengue. N Engl J Med 366:1423–1432. https://doi.org/10.1056/NEJMra1110265.
14. Chakraborty A, Jusko WJ. 2002. Pharmacodynamic interaction of recombinant human interleukin-10 and prednisolone using in vitro whole blood lymphocyte proliferation. J Pharm Sci 91:1334–1342. https://doi.org/10.1002/jps.3000.
15. Crotty S, Maag D, Arnold JJ, Zhong W, Lau JY, Hong Z, Andino R, Cameron CE. 2000. The broad-spectrum antiviral ribonucleoside ribavirin is an RNA virus mutagen. Nat Med 6:1375–1379. https://doi.org/10.1038/82191.
16. Furuta Y, Takahashi K, Fukuda Y, Kuno M, Kamiyama T, Kozaki K, Nomura N, Egawa H, Minami S, Watanabe Y, Narita H, Shiraki K. 2002. In vitro and in vivo activities of anti-influenza virus compound T-705. Antimicrob Agents Chemother 46:977–981. https://doi.org/10.1128/AAC.46.4.977-981.2002.
17. Maag D, Castro C, Hong Z, Cameron CE. 2001. Hepatitis C virus RNA-dependent RNA polymerase (NS5B) as a mediator of the antiviral activity of ribavirin. J Biol Chem 276:46094–46098. https://doi.org/10.1074/jbc.C100349200.
18. Nagata T, Lefor AK, Hasegawa M, Ishii M. 2015. Favipiravir: a new medication for the Ebola virus disease pandemic. Disaster Med Public Health Prep 9:79–81. https://doi.org/10.1017/dmp.2014.151.
19. Detje CN, Meyer T, Schmidt H, Kreuz D, Rose JK, Bechmann I, Prinz M, Kalinke U. 2009. Local type I IFN receptor signaling protects against virus spread within the central nervous system. J Immunol 182:2297–2304. https://doi.org/10.4049/jimmunol.0800596.
20. Matheron S, d'Ortenzio E, Leparc-Goffart I, Hubert B, de Lamballerie X, Yazdanpanah Y. 2016. Long-lasting persistence of Zika virus in semen. Clin Infect Dis 63:1264.
21. Nicastri E, Castilletti C, Liuzzi G, Iannetta M, Capobianchi MR, Ippolito G. 2016. Persistent detection of Zika virus RNA in semen for six months after symptom onset in a traveller returning from Haiti to Italy, February 2016. Euro Surveill 21(32):30314. https://doi.org/10.2807/1560-7917.ES.2016.21.32.30314.
22. Ku JH, Kim YH, Jeon YS, Lee NK. 1999. The preventive effect of systemic treatment with interferon-alpha2B for infertility from mumps orchitis. BJU Int 84:839–842. https://doi.org/10.1046/j.1464-410x.1999.00273.x.
23. Gallegos KM, Drusano GL, D'Argenio DZ, Brown AN. 2016. Chikungunya virus: in vitro response to combination therapy with ribavirin and interferon alfa 2a. J Infect Dis 214:1192–1197. https://doi.org/10.1093/infdis/jiw358.
24. Brown AN, Bulitta JB, McSharry JJ, Weng Q, Adams JR, Kulawy R, Drusano GL. 2011. Effect of half-life on the pharmacodynamic index of zanamivir against influenza virus delineated by a mathematical model. Antimicrob Agents Chemother 55:1747–1753. https://doi.org/10.1128/AAC.01629-10.
25. Beal SL. 2001. Ways to fit a PK model with some data below the quantification limit. J Pharmacokinet Pharmacodyn 28:481–504. https://doi.org/10.1023/A:1012299115260.
26. Madelain V, Guedj J, Mentre F, Nguyen TH, Jacquot F, Oestereich L, Kadota T, Yamada K, Taburet AM, de Lamballerie X, Raoul H. 2017. Favipiravir pharmacokinetics in nonhuman primates and insights for future efficacy studies of hemorrhagic fever viruses. Antimicrob Agents Chemother 61:e01305-16. https://doi.org/10.1128/AAC.01305-16.
27. Bulitta JB, Okusanya OO, Forrest A, Bhavnani SM, Clark K, Still JG, Fernandes P, Ambrose PG. 2013. Population pharmacokinetics of fusidic acid: rationale for front-loaded dosing regimens due to autoinhibition of clearance. Antimicrob Agents Chemother 57:498–507. https://doi.org/10.1128/AAC.01354-12.
28. Bulitta JB, Bingolbali A, Shin BS, Landersdorfer CB. 2011. Development of a new pre- and post-processing tool (SADAPT-TRAN) for nonlinear mixed-effects modeling in S-ADAPT. AAPS J 13:201–211. https://doi.org/10.1208/s12248-011-9257-x.